ADVANCED FUNCTIONAL MATERIALS
www.afm-journal.de

Confined Sulfur in Microporous Carbon Renders Superior Cycling Stability in Li/S Batteries

Yunhua Xu, Yang Wen, Yujie Zhu, Karen Gaskell, Katie A. Cychosz, Bryan Eichhorn, Kang Xu,* and Chunsheng Wang**

The use of sulfur in the next generation Li-ion batteries is currently precluded by its poor cycling stability caused by irreversible Li_2S formation and the dissolution of soluble polysulfides in organic electrolytes that leads to parasitic cell reactions. Here, a new C/S cathode material comprising short-chain sulfur species (predominately S_2) confined in carbonaceous subnanometer and the unique charge mechanism for the subnano-entrapped S_2 cathodes are reported. The first charge–discharge cycle of the C/S cathode in the carbonate electrolyte forms a new type of thiocarbonate-like solid electrolyte interphase (SEI). The SEI coated C/S cathode stably delivers ≈600 mAh g^{-1} capacity over 4020 cycles (0.0014% loss $cycle^{-1}$) at ≈100% Coulombic efficiency. Extensive X-ray photoelectron spectroscopy analysis of the discharged cathodes shows a new type of S_2 species and a new carbide-like species simultaneously, and both peaks disappear upon charging. These data suggest a new sulfur redox mechanism involving a separated Li^+/S^{2-} ion couple that precludes Li_2S compound formation and prevents the dissolution of soluble sulfur anions. This new charge/discharge process leads to remarkable cycling stability and reversibility.

1. Introduction

Implementation of renewable energy sources at large scales, such as solar, wind, or ocean/river waves, requires integrated energy storage units of large capacity, high rate capability, high efficiency, long cycle life, nontoxicity, and low cost.[1,2] Current state-of-the-art Li ion batteries fail to meet this host of requirements, as demonstrated by the performance of its flagship chemistry $LiCoO_2$. Despite its widespread implementation, $LiCoO_2$ is toxic, expensive (≈\$20 kg^{-1}), and typically characterized by mediocre capacity (≈150 mAh g^{-1}) due to intrinsic limitations imposed by the inert intercalation hosts.[2–4] This latter limitation is expected to be broken only with cathode materials of the "conversion-reaction" nature,[4] and elemental sulfur has been considered a promising candidate, due to its abundant distribution in the earth's crust, commodity availability at \$0.05 kg^{-1}, projected theoretical capacity of 1672 mAh g^{-1}, and low toxicity.[5–9] In particular, numerous studies have been conducted on the possible coupling of sulfur-based cathode materials with lithium that could provide energy densities above 500 Wh Kg^{-1} at the device level.[10–39]

The major obstacle preventing implementation of sulfur based cathodes is the poor cycling stability resulting from the formation of polysulfides (Li_2S_n, $n \geq 4$) during the reduction of elemental sulfur, and their subsequent parasitic reactions with the anode. This parasitic shuttle reaction results in rapid capacity fading, low Coulombic efficiency, high self-discharge, and the eventual loss of active materials due to the insulating natures of the final discharged products Li_2S. An effective strategy to minimize these parasitic reactions is to immobilize the redox active sulfur species inside the nanostructures of carbonaceous hosts[10–23] or to shelter the sulfur with electronically conductive coatings such as graphene sheets or polymers.[24–26] However, since these designed nanostructures remain partially open, the polysulfides are not completely sequestered but are instead still in partial contact with the bulk electrolyte. This strategy has resulted in slower cycling degradation due to the retarded dissolution and migration of these polysulfide species but degradation persists in all of these systems.

The generation of polysulfides can be prevented by restricting the voltage range of the sulfur cathode to cycle in the region of 1.7 to ≈2.30 V (or simply applying a capacity limit of 700 or 1000 mAh g^{-1}), in which only the insoluble low-order polysulfide reaction is utilized. This limited cycling precludes polysulfide formation and increases stability to the order of ≈500 cycles.[27] However, this strategy significantly reduces the potential capacity with only a modest increase in cycle life.

Dr. Y. Xu, Dr. Y. Wen, Dr. Y. Zhu, Prof. C. S. Wang
Department of Chemical and Biomolecular Engineering
University of Maryland
College Park, MD 20742, USA
E-mail: cswang@umd.edu
Dr. K. Gaskell, Prof. B. Eichhorn
Department of Chemistry and Biochemistry
University of Maryland
College Park, MD 20742, USA
E-mail: eichhorn@umd.edu
Dr. K. A. Cychosz
Quantachrome Instruments
1900 Corporate Drive
Boynton Beach, FL 33426, USA
Dr. K. Xu
Electrochemistry Branch
Power and Energy Division Sensor and
Electron Devices Directorate
U.S. Army Research Laboratory
Adelphi, MD 20783, USA
E-mail: conrad.k.xu.civ@mail.mil

DOI: 10.1002/adfm.201500983

In addition to the sulfur chemistry, electrolytes also significantly impact the electrochemical performance of Li–C/S systems. Carbonate solvents react with polysulfides, forming excessive solid electrolyte interphase (SEI) species. These irreversible reactions both consume active sulfur material and constitute an additional barrier to reaction kinetics as reflected by low capacity and poor rate capability.[28–30] However, the formed SEI mitigates the shuttling reaction of the polysulfides. In contrast, ether-based electrolytes, in which polysulfides are highly soluble, render higher capacity utilization of active sulfur and faster kinetics, but they also facilitate parasitic shuttling reactions. When the advantages and disadvantages of these electrolyte systems are weighed, the ether-based electrolytes are often chosen in favor of their carbonate-based counterparts.

It has been demonstrated that confining short-chain species such as S_4 and S_2 in carbonaceous pores of varying sizes significantly reduces the parasitic reactions but does not eliminate them entirely.[10–23] It seems that the formation of higher-order polysulfides in those cases is suppressed simply due to the physical restriction imposed by the narrow environment inside the carbonaceous host; however, no fundamental understanding has been gained regarding the behavior of those sulfur species under both electrochemical and spatial constraints. We describe here the successful entrapment of S_2 species inside the 0.5 nm pores of a carbon host that is capped with new type of thiocarbonate-like SEI. Unlike previous C/S cathode systems, this electrode is remarkably stable to full charge/discharge in carbonate based electrolytes and has delivered ≈600 mAh g^{-1} capacity for over 4000 cycles at almost quantitative (≈100%) Coulombic efficiency during a two-year test. Extensive X-ray photoelectron spectroscopy (XPS), X-ray diffraction (XRD), electrochemical and vibrational (IR and Raman) studies suggest that the C/S cathode undergoes a new type of discharge mechanism that might involve the formation of separated S^{2-} and Li^+ ions. The combination of subnanoconfinement and SEI capping of the S_2 moieties inside the pores precludes the formation of bulk Li_2S that characterize traditional lithiation reactions.

2. Results and Discussion

Microporous carbon with subnanometer cavities was prepared according to literature methods[12] and was used as a host to immobilize the active sulfur species. The porous structure of the microporous carbon was analyzed using CO_2 adsorption (Figure S1, Supporting Information). The pore volume and porosity were calculated to be 0.217 cm^3 g^{-1} and 33%, respectively. The majority of the pores were distributed within a narrow range near 0.5 nm, which can only accommodate short-chain S_2 (≈0.4 nm in diameter) but not the larger molecules of S_{3-8} (>0.5 nm).[16] However, a small portion (<10%) of larger pores do exist, which could accommodate S_{3-8} or high order polysulfides.

Carbon/sulfur mixtures with weight ratios of 80/20, 60/40, 40/60, and 20/80 were used to make the C/S composites of varying sulfur loading. The mixtures were heated at 600 °C, where the elemental sulfur dissociates into S_2 in the gas phase,[40] which was then infused into the carbon micropores at low pressure. By comparing the weight of the carbon substrate before and after thermal impregnation, the actual sulfur contents of the final products were determined to be 15%, 31%, 55%, and 75%, and hereafter denoted as S15, S31, S55, and S75, respectively. The actual composition of S31 was further confirmed with thermal gravimetric analysis in Figure S2 (Supporting Information) (31% S, 69% C). While the S_2 molecules that are physically entrapped inside the subnanometer cavities remain stabilized and are prevented from reforming S_8 or high order polysulfur species upon cooling, the S_2 molecules deposited on the carbon surface (i.e., outside of the micropores) or residing in larger pores presumably convert back to S_8 at room temperature. We denote the former as "interior sulfur" and the latter "exterior sulfur."

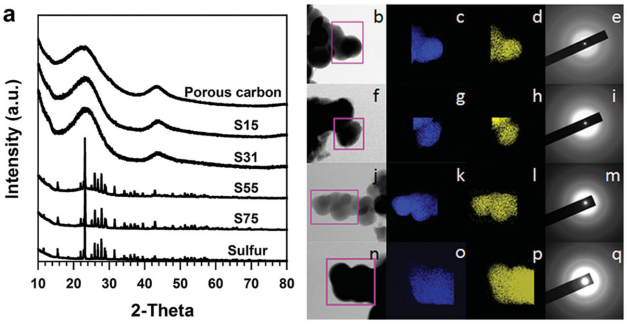

Figure 1. a) XRD patterns of microporous carbon, pristine sulfur, and C/S nanocomposites with varying sulfur loadings. TEM images in (b,f,j,n), corresponding elemental mapping for carbon in (c,g,k,o) and sulfur in (d,h,l,p), and SAED images in (e,i,m,q) for S15 (b–e), S31 (f–i), S55 (j–m), and S75 (n–q).

The XRD patterns for these nanocomposites are compared against elemental sulfur (S_8) and the microporous carbon host in **Figure 1**a. Well-defined characteristic diffraction peaks of S_8 are present in the high sulfur-loaded nanocomposites (S55 and S75), presumably formed from S_2 fragments that recombined on the carbon surface or in larger pores. However, crystalline S_8 is clearly absent in the low-sulfur composites (S15 and S31), indicating that only small-chain fragments or amorphous S_8 deposits are present.

The transmission electron microscopy (TEM) images and elemental mapping images shown in Figure 1b–q illustrate that sulfur (Figure 1d,h,l,p) is distributed homogenously throughout the carbon host in all cases. The selected area electron diffraction (SAED) performed on the four different C/S composites show only broad diffraction rings (Figure 1e,i,m,q), indicating the presence of noncrystalline sulfur distributed throughout the microporous carbon. The crystalline S_8 detected by XRD in S55 and S75 (Figure 1a) most likely sublimes off from the sample under the high vacuum conditions of TEM experiment, while the noncrystalline sulfur detected by TEM in all four C/S samples is attributed to the S_2 molecules within the 0.5 nm micropores and other noncrystalline sulfur fragments that are stabilized in the larger pores (Figure 1d,h,i,p). The exterior S_8 molecules appear to sublime under high vacuum whereas the entrapped S_2 and other short chain sulfur fragments interact strongly with carbon host and persist in the high vacuum TEM environment. The fact that these short-chain sulfur species can be imaged with TEM serves as convincing evidence for how strongly these interior sulfur species interact with the carbon

Adv. Funct. Mater. 2015,
DOI: 10.1002/adfm.201500983

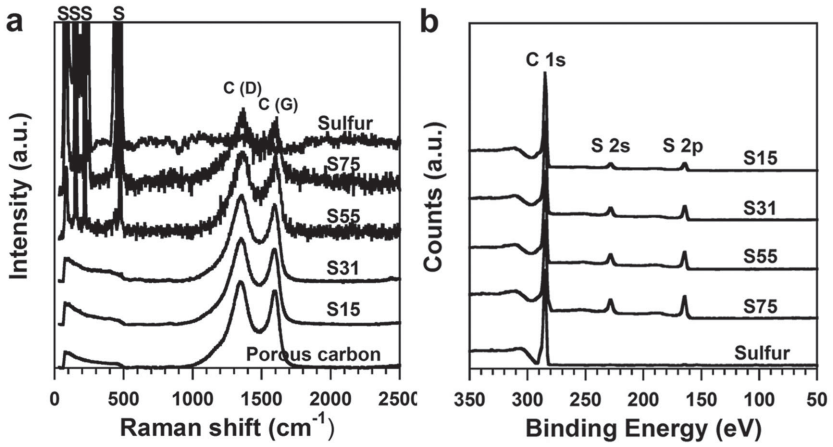

Figure 2. a) Raman and b) X-ray photoelectron spectra (XPS) of pristine sulfur, microporous carbon host, and C/S nanocomposites varying sulfur loadings. Based on the peak area of XPS figure in (b), the S2 confined inside the carbon pores was calculated to be 15 wt% for S31.

host, as surface-physisorbed sulfur would not survive such high vacuum (<10^{-6} Pa) employed in these experiments.

The differences between the various C/S nanocomposites are further demonstrated by the Raman spectra as shown in **Figure 2**a, where microporous carbon and pristine S_8 again serve as references. The two peaks are observed at 1350 and 1580 cm^{-1} for the carbon host corresponding to disordered (D) and graphitic (G) modes of carbon, respectively, revealing its partial graphitic nature. A characteristic collection of sharp peaks below 500 cm^{-1} associated with the strong S—S vibrational modes with large Raman cross sections are observed for the pristine S_8 sample as well as high sulfur-loading nanocomposites (S55 and S75). However, these peaks are absent for S15 and S31 composites, in agreement with XRD observation that only negligible amount of exterior sulfur exists in S15 and S31 composites (Figure 1a). While all S—S vibrational modes typically give strong Raman signals in the 100–500 cm^{-1} range, S_x species (e.g., S_x polymers) confined inside of carbon hosts, such as carbon nanotubes, do not generate such S—S Raman signals.[31]

The distribution of different sulfur species in the C/S composites was further examined with XPS, where pristine S_8 on carbon tape served as reference (Figure 2b). In the XPS experiments, all samples were evacuated to ≈5×10^{-6} Pa at room temperature, where pristine cyclic S_8 completely sublimes as in TEM experiments. The control S_8 reference XPS data were therefore conducted at –120 °C (Figure S3, Supporting Information) where sublimation is retarded. However, strong XPS sulfur 2p peaks are observed for all of the C/S composites at room temperature, demonstrating that it is immobilized in the carbonaceous micropores even under the ultrahigh vacuum (UHV).

Among the C/S nanocomposites, S31 stands out in terms of excellent electrochemical reversibility (see below). To understand the origin of its superior behavior, we evaluated how much sulfur was actually confined in the subnanometer cavities versus how much remained at the surface or in larger pores as exterior sulfur among the different composites. XPS can effectively differentiate between relative concentrations of "interior" versus "exterior" sulfur species due to the fact that photoelectrons originating from deeper within the sample will more likely suffer inelastic collisions resulting in an increase in background to the lower kinetic energy side of the photoelectric peak, whereas photoelectrons from the surface sulfur will suffer fewer or no collisions and thus contribute a larger proportion to the photoelectric "peak."[41] Hence, the distribution ratio (D) of these two different forms of sulfur can be derived from the ratio of photoelectric peak area ($I_{S\ 2p}$) and the increase in the background signal (B)

$$D = I_{S2p}/B \tag{1}$$

where the linear background B was taken between binding energies of 160 and 200 eV, and $I_{S\ 2p}$ encompasses the S 2p electrons as shown in Figure S4a (Supporting Information). The ratio D is a semiquantitative measure of the relative amount of "exterior" versus "interior" sulfur species as illustrated in **Figure 3**. Note that "exterior" sulfur described here refers to weakly trapped S_x species that are stable enough to survive UHV XPS analysis (i.e., not physisorbed S_8) but will still be exposed to electrolyte in a cell configuration. They are most likely S_x existing near the surface of the micropores or in the larger pores of ≈0.8 nm, where the spatial constraints may allow the partial reformation of larger sulfur oligomers upon cooling. The ratios obtained for the C/S composites are plotted in Figure S4b (Supporting Information) against the corresponding overall sulfur loadings. It is immediately apparent that S31, with the smallest D ratio (1.36), stands out uniquely from the rest of the nanocomposites. This minimum in D value indicates a greater amount of photoelectrons escaping from the deeper region under the surface, indicating a larger amount of confined sulfur as compared with exterior sulfur.

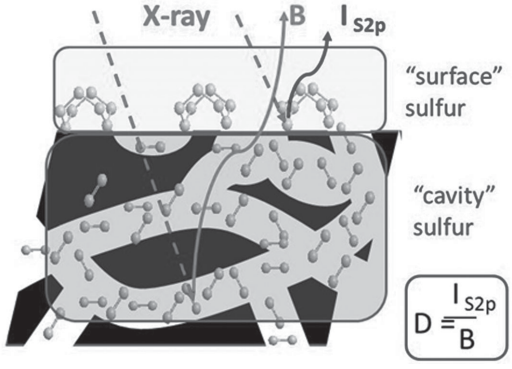

Figure 3. Schematic illustration of a) how distribution of "cavity" versus "exterior" sulfur was determined by S 2p XPS, and b) the rationale for different D values found in C/S nanocomposites at varying S/C ratios. Note that "cavity" sulfur confined deep in the carbon host largely (but not exclusively) contributes to the background (B), while "exterior" sulfur dominates the peak height (I S 2p).

What seems counter-intuitive is that, although S55 and S75 are more sulfur-rich than S15, their *D* values are comparable. Further examination reveals that in S15, amounts of both exterior and interior sulfur are low, while in S55 and S75, both amounts are high, leading to similar ratios of these three sulfur species (Figure S4b, Supporting Information). As a reference the *D* ratio calculated from the control S_8 sample (Figure S4, Supporting Information) was 1.7, this is comparable to the values of 1.65–1.85 found for S15, S55, and S75 samples reflecting the more homogeneous distribution of interior versus exterior sulfur.

In this sense, S31 is unique among all the composites made because of its higher relative amount of confined sulfur species, as schematically illustrated in Figure 3 and Figure S4c (Supporting Information). S31 appears to provide the optimal C/S cathode composition for the microporous carbon with porosity of 33%, because S15 provides insufficient active material, while excessive amounts of exterior sulfur in S55 and S75 induces parasitic processes responsible for rapid capacity fading.

Electrochemical tests were carried out on these model C/S composites in cathode-half cells using lithium as a counter anode in the voltage range of 3.0–1.0 V. Two different electrolytes, one based on carbonate (1 M $LiPF_6$ in ethylene carbonate (EC)/diethyl carbonate (DEC) 1:1 by volume) and the other on ether (1 M lithium bis(trifluoromethylsulfonyl)imide (LiTFSI) in tetra(ethylene glycol) dimethyl ether (TEGDME)), were employed to evaluate cycling stability. The voltage profiles of four C/S composites in these two electrolytes are displayed in Figure S5 (Supporting Information) for the first (Figure S5a,b, Supporting Information) and the second (Figure S5c,d, Supporting Information) cycles, respectively. The electrolytes make little difference to the low sulfur-loading nanocomposites S15 and S31 in the first cycles, as both displayed very short plateaus at 2.44 V and long discharge plateaus at 1.5–1.7 V, with corresponding charge plateaus at 1.8–2.0 V. The plateaus at 2.44 and 2.1 V, which are characteristic of the formation of high-order polysulfides (Li_2S_x, $x \geq 4$) and low-order polysulfides (Li_2S_x, $x < 4$), respectively, are absent in the second cycles in the carbonate electrolyte (Figure S5c, Supporting Information) or significantly diminished in the ether electrolyte (Figure S5d, Supporting Information).

In contrast, significant electrolyte effects are found for the high sulfur-loading composites S55 and S75. In addition to the "trapped S_2" plateau at 1.5–1.7 V, plateaus corresponding to low- and high-order polysulfides are prominent in the ether-based electrolyte at 2.1 and 2.4 V, respectively. These plateaus arise from the redox cycling of nonconfined exterior S_x in these composites. This polysulfide redox process results in a higher capacity; however, their dissolution and shuttling result in the slow but steady capacity fading, which precludes their use for rechargeable electrochemical energy storage devices. In carbonate electrolytes, these 2.4 and 2.1 V processes are absent, which is attributed to the reaction of polysulfides with the carbonate solvent molecules. The nucleophilic addition of the polysulfides to the carbonyl moieties in the alkylcarbonate solvents yields thiocarbonyls that form SEI layers and are redox-inactive.[28] This chemistry is discussed in the next section.

Of particular interest is the voltage plateau at lower potentials (1.5–1.7 V, depending on cell polarization) for the S15, S31, and S55 composites in both carbonate- and ether-based electrolytes. We attribute these processes to the redox cycling of short-chain sulfur that is confined within subnanometer cavities. Due to the high stability and solubility of high-order polysulfides in ether-based electrolytes, both free $S_2^{-1/-2}$ (reduction product of dissolved high-order polysulfides) and confined $S_2^{-1/-2}$ exist in S15, S31, and S55 composites when cycled in ether-based electrolytes. The reduction of free S_x ($2 \leq x \leq 4$) is attributed to the 2.1 V plateau and the reduction of the confined S_2 should be associated with 1.7 V plateau (Figure S5b,d, Supporting Information). For S31, the capacity of confined S_2 at 1.5–1.7 V is extremely reversible in carbonate-based electrolyte, although the capacity delivered by this process after the second cycle is only 660 mAh g^{-1} calculated based on the overall amount of sulfur loaded in the synthesis (31 wt%). This 31% contains a significant portion of partially stabilized exterior S_8 that is exposed to the electrolytes and ultimately forms electrochemically inactive SEI films. Therefore, evaluation of the capacity based on the total sulfur is an underestimate of the redox-active sulfur in the composite. Since we do not quantitatively know how much of the sulfur is sacrificed in SEI formation, it is difficult to provide an accurate capacity number. However, the S_2 confined inside the carbon pores was estimated to be 15 wt% by XPS experiments (Figure 3), in which the surface S_8 sublimed off in high vacuum. If the confined S_2 is taken as the only active sulfur, the capacity of active sulfur for S31 is then recalculated to be 1416 mAh g^{-1}, which is close to the theoretical capacity of 1673 mAh g^{-1}.

The remarkable electrochemical reversibility of the S31 composite is illustrated in **Figure 4**, where it was charged/discharged in cathode half cells between 1.0 and 3.0 V at a current density of 80 mA g^{-1} (0.1 C as evaluated with nominal 1 C = 800 mA g^{-1}) for the first 100 cycles, and then at a higher rate of 400 mA g^{-1} (0.5 C). After 2020 and 4000 cycles, respectively, the current was changed back to 80 mAh g^{-1} for 20 cycles each to check the sulfur utilization level. During the test of more than two years, there was negligible capacity loss observed for this S_2-dominated C/S_2 nanocomposite over 4020 cycles, with the loss rate of 0.0014% per cycle (Figure 4a). To our knowledge, this is the best cycling stability and the longest cycle numbers ever achieved for any Li/S system, and is comparable to or even better than that of commercial graphite anodes. Compared with the 10^2 cycles typically described in literature, the cycle life demonstrated here represents a revolutionary leap, because the parasitic nature of Li/S chemistry has been fatal to the long calendar life (>10 years, >1000 cycles) required by large-scale applications such as automotive or grid-storage applications, which require the loss of the limiting active species to be below 0.01% per cycle (i.e., $(0.9998)^{1000} = 0.82$, with 80% capacity retention widely adopted by battery industry as life-termination line).[42]

Behind this excellent cycling stability was the nearly quantitative Coulombic efficiency in each cycle, with the exception of the initial cycles where irreversible capacity was consumed by interphase formation as well as irreversible reaction between exterior sulfur and carbonate molecules. The rate capability of S31 in carbonate-based electrolyte was also evaluated using higher current densities as shown in Figure 4b. ≈255 mAh g^{-1} is retained at the rather high rate of 4800 mA g^{-1} (equivalent of 6 C), reflecting the fast kinetics of the system.

Adv. Funct. Mater. **2015**,
DOI: 10.1002/adfm.201500983

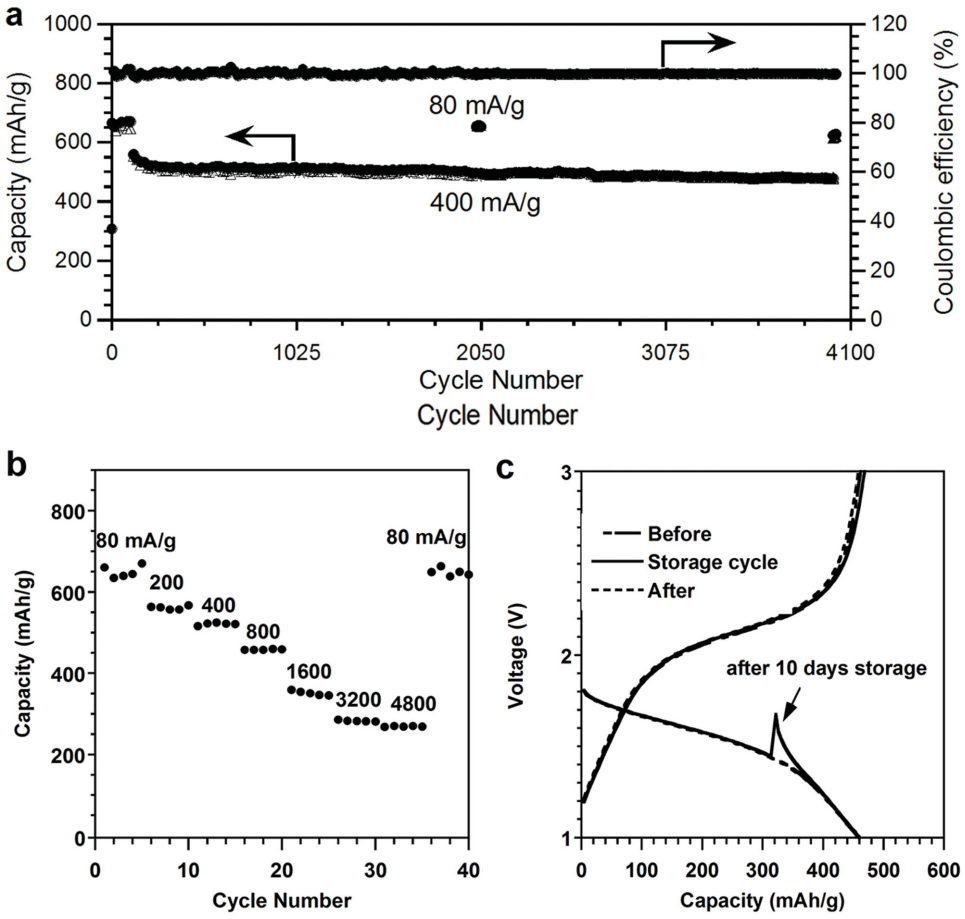

Figure 4. Electrochemical performance of S31 nanocomposite in carbonate-based electrolyte (1 M $LiPF_6$ in EC:DMC (v:v = 1:1)). a) Cycling stability and Coulombic efficiency measured at 400 mA g^{-1} (0.5 C), with the exceptions for the first 100 cycles and the 20 cycles after the 2020th and 4000th cycle, respectively, where a lower rate 80 mA g^{-1} (0.1 C) was used. b) The storage test, during which the cell was kept at 70% state-of-charge (1.5 V) for 10 d before resuming cycling. c) The rate capability at various current densities from 80 (0.1 C) to 4800 mA g^{-1} (6 C).

The exceptional cycling stability indicates that the dissolution and shuttling reactions of polysulfide species have been eliminated. In typical Li/S cells, dissolution and diffusion of high-order polysulfides induce both reversible and irreversible capacity loss. The Li_2S deposition on the Li anode consumes the active sulfur materials, leading to an irreversible capacity loss, while the shuttle reaction creates an internal short, leading to capacity loss that may be recoverable. Both parasitic processes contribute to low Coulombic efficiencies. Upon storage, the consequences of these parasitic reactions become more pronounced, and the shuttling effects can be probed by monitoring the open-circuit voltage (OCV) of an Li–S cell and the overall capacity loss is normally evaluated by testing the retained capacity after storage using a cycled (activated) Li/S cell.[43] In this work, we performed storage tests to reveal the self-discharge level, in which S31 half cathode cells at fresh state and 70% state-of-discharge were stored at room temperature for ten days (Figure S6, Supporting Information and Figure 4c). The constant OCV and ensuing discharge profile of the cell was virtually identical to the previous and subsequent cycles, confirming that shuttling of polysulfides is essentially nonexistent. To further confirm the absence of the self-discharge, the storage was conducted in a four month (≈120 days) period at 90% of state-of-charge. Again, the charge/discharge profiles before and after the storage test are virtually identical (Figure S7, Supporting Information). The effective elimination of polysulfide shuttling that has been plaguing Li/S systems further suggests that these interior short-chain sulfur species are not only stabilized, but physically sequestrated inside the 0.5 nm cavities of the microporous carbon host. We believe that C/S_2 has different lithiation mechanism and unique SEI layer plays an essential role as discussed below.

XPS analysis was performed on S31 nanocomposites that were cycled in carbonate electrolyte and then recovered at a discharged state (1.0 V). The corresponding spectra are shown in **Figure 5**. All spectra were referenced to the hydrocarbon signal at 284.8 eV. In the C 1s spectra, a series of signals were identified at 290, 288.2, 286.5, 284.8, and 283.2 eV (Figure 5a). The peak at 284.8 eV is attributed to both hydrocarbon and the elemental carbon in the microporous carbon host, and those at 290 and 286.5 eV are assigned to carbonate and alkoxy subunits, arising from Li_2CO_3, alkylcarbonates, and polyether that are often found in the SEI of Li ion battery electrodes.[44,45] However, the peaks at 288.2 and 283.2 eV represent new chemical

ADVANCED FUNCTIONAL MATERIALS
www.afm-journal.de

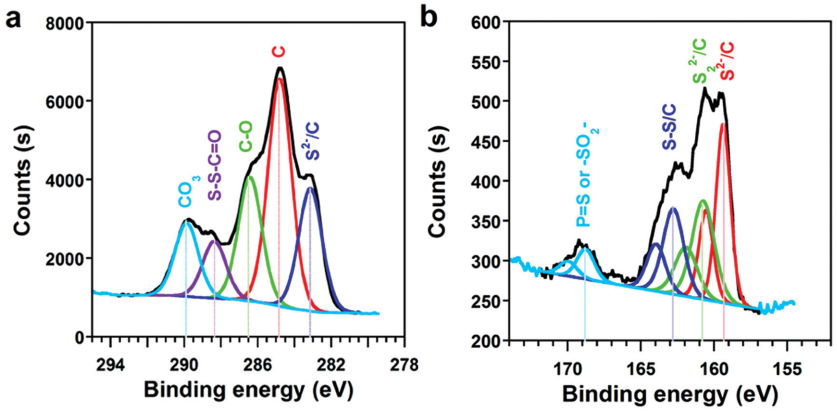

Figure 5. XPS a) C 1s and b) S 2p spectra for S31 nanocomposites at discharged state (1.0 V) after being cycled in carbonate-based electrolytes. The dashed plots represent the overall counts of photoelectrons detected, while the deconvoluted peaks were plotted in solid lines.

species that have never been reported to our knowledge. Repeated experiments were conducted to confirm that these signals are not the result of instrumental artifacts. The 288.2 eV signal corresponds to a carbon state whose electron-deficiency lies between a carbonyl (C═O) and a carboxyl (COOR), and the 283.2 eV signal is similar to a carbide (C^-) species bearing extra negative charge.[46] We tentatively assign the electron-deficient carbon to be the product of the nucleophilic reaction between short-chain sulfur and carbonate molecule at low potential. The proposed thiocarbonate-like species could result from the following process[28]

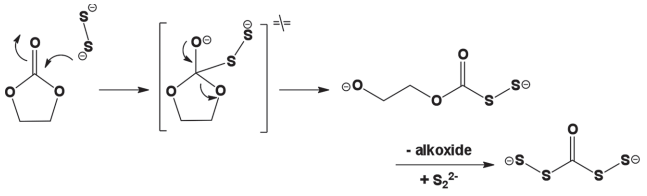

This new compound is a prominent component of the formed SEI, along with the familiar alkylcarbonate (CO_3^{2-}) and polyether (C—O) species. These species are all formed in an irreversible process during the first cycle of the cell.

In contrast, the carbide-like species at 283.2 eV is directly dependent on the state-of-charge of the C/S_2 composite, enriched at discharged state when sulfur was reduced to sulfides (S_2^{2-} or S^{2-}) and diminished when sulfides were oxidized back to S_2 (Figure S8a, Supporting Information). In comparison, this carbide-like peak is 1.0 eV lower in energy than that of pristine graphite (284 eV) and 1.8 eV lower than the C 1s peaks for a fully lithiated graphite (Li_xC_6, 285 eV).[47] Since the C/S_2 cathodes were discharged to 1.0 V, which is too high even for the formation of high-stage lithiated graphite,[48,49] we believe that this peak is not due to Li^+ intercalation into the carbon host. Instead, it is indicative of an interaction between the carbon host and an anion. We attribute this carbide-like species to the chemical interaction between the confined sulfide anion and carbon host, where a stabilizing partial charge transfer occurs between the undercoordinated sulfide anion (see below) and the graphitic carbon host.

The corresponding S 2p spectra (Figure 5b) were fit with spin–orbit coupled 2p 3/2 and 2p 1/2 doublets, constrained at 1.18 eV separation with a characteristic 2:1 area ratio and equal full-width at half maximum. The peak envelope required four pairs of doublets to yield a good fit.[46] Such fitting placed these 2p 3/2 peaks at 168.8, 162.8, 160.8, and 159.3 eV, respectively. The 162.8 and 160.8 eV peaks are attributed to short-chain sulfur (S_2) and sulfide (S_2^{2-}), with some negative shift (–0.9 to –1.6 eV) in binding energy as compared with the typical terminal (162.4 eV) and nonterminal sulfides (163.7 eV).[50] However, the peaks at 168.8 and 159.3 eV are unique sulfur species that have not been previously reported to the best of our knowledge. Again, we excluded the possibility of artifacts by reproducing these signals with duplicate samples. The most electron-deficient sulfur (168.8 eV) should usually correspond to high valence sulfur species such as sulfone or sulfate (168–170 eV), but the possibility of their formation should be excluded here because, given the potential range employed in the work (1.0–3.0 V vs Li) where the electrochemical oxidation of sulfur into S═O is unlikely. We believe that this peak should arise from the reaction between sulfide and PF_6^- anion, because thiophosphate species (P═S) also fall in the same range of binding energies.[46] This species, arising from either complete or incomplete substitution of F by sulphide and as represented by the general formula of PS_xF_y, should also remain part of the SEI, as confirmed by Figure S8b (Supporting Information) when the nanocomposite is brought back to charged state.

The new S 2p peak at 159.3 eV represents an extremely electron-rich sulfur species whose binding energy is even lower than that of S^{2-} in bulk Li_2S (≈161.0 eV) by 1.7 eV. Since it coexists with the carbide-like species in the C 1s spectra (Figure 5a) and also disappears upon charging (Figure S8b, Supporting Information), we believe that both peaks arise from the same species. The data are consistent with an undercoordinated sulfide ion that is sharing negative charge with the mesoporous carbon host. The shared formal negative charge leads to anomalously low binding energies for both C 1s and S 2p electrons. Thus, the C 1s and S 2p XPS data together strongly suggest that a new sulfide species is created and this species is integral to the reversible sulfur redox cycling in the cell. This new chemical state of sulfide differs from those reported in literature[11,14,15,23–26,38] in that complete ion pairing between S^{2-} and Li^+ to form Li_2S might be precluded by the size constraints of the carbon pores and the presence of the SEI layer coating the C/S cathode. Because the confined S^{2-} is not Coulombically stabilized by Li^+ ions in the same manner as in bulk Li_2S, the S^{2-} electrons are in a very high energy state that gives rise to the anomalously low S 2p binding energies. The high energy S^{2-} electrons are partially stabilized through charge sharing with carbon host, which gives rise to the carbide-like species observed in the C 1s spectra, as discussed below.

The combined structural and spectroscopic evidence described above indicate that the C/S nanocomposites

DOI: 10.1002/adfm.201500983

described here contain S_2 molecular species entrapped in the ≈0.5 nm cavities of the microporous carbon host. These short-chain fragments are the predominate active forms in the S15 and S31 composites while the S55 and S75 composites contain both confined S_2 and exterior crystalline S_8, with the latter distributed on the carbon surfaces and the larger pores ≈0.8 nm. The S31 composite represents the optimum scenario for the microporous carbon used in this work, in which all the sub-nano-cavities are saturated with S_2 with relatively lower quantities of exterior sulfur. This small amount of surface sulfur is consumed by the electrolyte to form an adventitious, thin SEI capping layer, which serves as an additional barrier to prevent parasitic shuttling that often plagues the electrochemistry of Li/S batteries.

It is well known that the stable sulfur allotrope at room temperature, cyclo-S_8, readily fragments at elevated temperatures into gaseous acyclic short-chain fragments, where the chain length decreases with increasing temperature.[40] Diatomic S_2 is a prominent species at 600 °C and low total pressure, but spontaneously converts back to S_8 upon cooling to room temperature. While it has been proposed that S_2 species could be stabilized in a host matrix at room temperature,[40] we show here that gas phase impregnation S_2 into the ≈0.5 nm cavities of microporous carbon, coupled with a thin SEI capping layer, prevents the reoligomerization of metastable S_2 to produce a remarkably efficient and stable cathode material for Li ion batteries.

The charge/discharge mechanism of the C/S_2 nanocomposite thus prepared is unique in that a new sulfur/sulfide species is involved in the cathodic electrochemical processes. The XPS data suggest that the "lithiation" of sulfur occurring with cell discharge proceeds by way of indirect ion pairing (Figure 5a,b and Figure S7a,b, Supporting Information). The reversible and simultaneous formation of low-binding-energy S^{2-} ions and carbide-like carbon hosts at the discharged state indicates that the lithiated sulfide (i.e., Li_2S) is not formed in the cathode in the traditional sense. In bulk Li_2S, a sulfide ion resides in a cubic hole surrounded by eight Li^+ cations, which stabilize the high negative charge on S^{2-} to give a corresponding 2p electron binding energy of 161 eV. In discharged S31, however, the absence of Li^+ stabilization in close vicinity leaves the S^{2-} ion in a higher energy state, which is revealed by the anomalously low S 2p electron binding energy (159.3 eV). To compensate for the excessive charge build-up, partial charge transfer occurs to the carbon matrix, giving rise to the carbide-like nature of the support. This unique charge/discharge chemistry with a sloping plateau between 1.5 and 1.7 V is also evident in charge/discharge curves of S15 and S31 composites in both carbonate- and ether-based electrolytes (Figure S5, Supporting Information), which contrasts the flat plateaus typically observed for molecular redox cycling of polysulfides on carbon electrodes at ≈2.1 V (Equation (2)).

$$Li_2S_4 + 6e^- + 6Li^+ \rightarrow 4Li_2S(s) \quad (2)$$

In the literature, the traditional charge/discharge process has been attributed to the lithiation reactions of free short-chain sulfur species (Li_2S_x, $x < 4$) to form insoluble sulfides Li_2S_2 and Li_2S. In our case, however, this lithiation process corresponds to a unique coupling between Li^+ and a charge-sharing matrix C/$2S^{2-}$ (Equation (3))

$$C/S_2 + 4e^- + 4Li^+ \rightarrow C/2S^{2-}/4(Li^+) \quad (3)$$

where C/$2S^{2-}$ is sulfide confined in the carbon cavity and /4(Li^+) are the delocalized charge compensating Li^+ ions. The strong association of S_2 with the carbonaceous host drives down its electrochemical potential from the normal flat plateau at 2.1 V of Li_2S_4 (corresponding to $Li_2S_4 + 2Li^+ + 2e^- \leftrightarrow 2Li_2S_2$ and $Li_2S_2 + 2Li^+ + 2e^- \leftrightarrow 2Li_2S$) to slope at 1.7–1.5 V for C/S_2. This reduction in potential is presumably due to the charge delocalization (i.e., electron coupling) between S and carbon host. Similar reductions of lithiation potentials have been observed previously in metal sulfides, for which the bonding between Ni, Fe, or Cu and S was believed to be responsible.[51–53]

With the higher sulfur loadings of the S55 and S75 composites, a different mechanism is involved and the effects of the electrolyte become apparent (Figures S5 and S9, Supporting Information). The low sulfur capacity utilization of S55 and S75 in carbonate-based electrolyte in Figure S9c (Supporting Information) is mainly caused by the side reactions between the dissolved polysulfides with carbonate electrolyte to form an excessively thick interphase consisting of thiocarbonates. The poor solubility of polysulfides in the carbonate electrolyte along with the electronically and ionically insulating nature of sulfur and low-order polysulfides (Li_2S and Li_2S_2) also contributed to the decreasing capacity utilization. On the other hand, the higher sulfur utilization of S55 and S75 in ether electrolyte (Figures S5b,c and S9d, Supporting Information) benefitted from the high solubility of their lithiated products, along with the fact that ether-based electrolytes are reductively stable against SEI formation on carbon host surface.[44] However, these merits will not last in long term. As mentioned above and reported extensively in literature, this high capacity is accompanied with the migration of these polysulfides toward and subsequent reduction at the anode surface. This deleterious shuttling is clearly evident in S75, which loses rechargeability within three cycles, and S55, which rapidly fades below 500 mAh g^{-1} (Figure S9d, Supporting Information). S31 stands out even in ethereal electrolyte, delivering a stable capacity of 700–750 mAh g^{-1} at nearly quantitative Coulombic efficiency (>99.5%), but at a higher fading rate (Figure S10, Supporting Information).

Although electrolytes play a key role in improving cell performance for Li–S systems,[54] it has been well recognized that no perfect solution exists for Li/S systems regarding the dilemma of "capacity utilization" versus "capacity fading." The former would require higher solubility of active sulfur for thorough accessibility and the latter would require the exact opposite for minimal shuttling. Although more complete sulfur utilization is realized in ethereal electrolytes, the fast capacity fading renders them impractical. On the other hand, carbonate-based electrolytes cannot dissolve short-chain sulfides and are chemically reactive toward polysulfide species.[29] However, the S31 C/S_2 composite described here successfully solves the "capacity fading" issue while still maintaining reasonable "capacity utilization" through sequestration and isolation of the redox active S_2 species. The mechanism identified in this work points to a new avenue of designing carbon/sulfur composites

by considering a complete sequestration of the latter with both spatial constraints and interphase formation. If the specific loading of sulfur-active species (mAh cm^{-2}), currently limited by the pore population of the microporous carbon host, could be raised to practical level, the perfect electrochemical reversibility of such systems will bring about transformational changes to the development of sulfur-based cathode materials for the next generation battery chemistry.

3. Conclusion

Through detailed structural, chemical, and morphological analyses, we reveal that a new sulfur chemistry has been created with the sequestration of short-chain sulfur species into subnanometer cavities and the charge delocalization between them and the carbonaceous host. This complete sequestration, assisted by a new type of SEI containing thiocarbonates, is responsible for the superior electrochemical reversibility as demonstrated by highly reversible capacities achieved at almost 100% Coulombic efficiency over 4020 cycles. This new charge/discharge mechanism opens up new possibilities for designing nanostructured cathode materials for rechargeable Li/S battery chemistry.

4. Experimental Section

Synthesis of Microporous Carbon: The microporous carbon was synthesized based on the previously reported method.[12] Sucrose was used as the carbon source. Typically, 20 g sucrose dissolved in 6 M sulfuric acid to form 5% sucrose solution, which was refluxed in 1 L round bottom flask at 120 °C for overnight. The resulting black suspension was filtered and washed with distilled water several times. The product was dried at 100 °C in oven for 24 h, and underwent carbonization at 1000 °C for 3 h with heating rate of 5 °C min^{-1} under argon/5% H_2 atmosphere.

Preparation of C/S Composites: Sublimed elemental sulfur (S_8) (Sigma-Aldrich, USA) was mixed thoroughly with microporous carbon at different C/S ratios of 80/20, 60/40, 40/60, and 20/80 by weight. The mixtures were sealed in glass tubes under vacuum and underwent heat-induced fragmentation at 600 °C for 5 h with heating ramp of 5 °C min^{-1}. The resulting C/S composites were collected after cooling down to room temperature.

Material Characterization: The porous structure of the microporous carbon was analyzed using CO_2 (at 273 K) adsorption on an Autosorb-iQ MP (Quantachrome Instruments, USA). The sample was outgassed under turbomolecular pump vacuum at 423 K for 12 h prior to the measurement. From the measured CO_2 isotherm, the micropore size distribution was calculated using non-local density functional theory (NLDFT) method and the micropore volume was calculated using the Dubinin–Radushkevich (DR) method in the P/P_0 range from $10e^{-4}$ to $10e^{-2}$. The elemental mapping imaging was conducted on JEOL (Japan) 2100F field emission TEM. XRD pattern was recorded by Bruker Smart1000 (Bruker AXS Inc., USA) using Cu Kα radiation. XPS spectra were collected on Kratos AXIS 165 spectrometer, using monochromatic Al Kα radiation (280 W) at room temperature for pure carbon and C/S composites, and at –120 °C for pure sulfur. Charge neutralization was required to minimize sample charging. Raman measurements were performed on a Horiba Jobin Yvon Labram Aramis using a 532 nm diode-pumped solid-state laser, attenuated to give ≈900 μW power at the sample surface.

Electrochemical Measurement: The microporous C/S composites were mixed with carbon black and sodium alginate binder to form a slurry at the weight ratio of 70:15:15. The electrode was prepared by casting the slurry onto aluminum foil using a doctor blade and dried in a vacuum oven at 60 °C overnight. With binder, the overall S content in the cathode is 21.7%, and the areal sulfur loading is 0.17 mg cm^{-2}. Cells were assembled with lithium as the counter electrodes, 1 M $LiPF_6$ in EC/DEC 1:1 by volume) or ether (1 M LiTFSI in TEGDME) as electrolyte, and Celgard 3501 (Celgard, LLC Corp., USA) as the separator. The amount of electrolytes used for each cell is about 0.1 mL for both carbonate and ether-based electrolytes. Electrochemical performance was tested using Arbin battery test station (BT2000, Arbin Instruments, USA). Capacity was calculated on the basis of the sulfur mass.

Supporting Information

Supporting Information is available from the Wiley Online Library or from the author.

Acknowledgements

This work was supported as part of the Nanostructures for Electrical Energy Storage (NEES), an Energy Frontier Research Center funded by the U.S. Department of Energy, Office of Science, Basic Energy Sciences under Award number DESC0001160.

Received: March 12, 2015
Revised: May 7, 2015
Published online:

[1] Z. Yang, J. Zhang, M. C. W. Kintner-Meyer, X. Lu, D. Choi, J. P. Lemmon, J. Liu, *Chem. Rev.* **2011**, *111*, 3577.
[2] B. Dunn, H. Kamath, J.-M. Tarascon, *Science* **2011**, *334*, 928.
[3] J. Amirault, J. Chien, S. Garg, D. Gibbons, B. Ross, M. Tang, J. Xing, I. Sidhu, P. Kaminsky, B. Tenderich, *The Electric Vehicle Landscape* University of California, Berkeley, CA **2009**.
[4] M. S. Whittingham, *Chem. Rev.* **2014**, *114*, 11414.
[5] A. Manthiram, Y. Fu, S. H. Chung, C. Zu, Y. H. Su, *Chem. Rev.* **2014**, *114*, 11751.
[6] P. G. Bruce, S. A. Freunberger, L. J. Hardwick, J.-M. Tarascon, *Nat. Mater.* **2012**, *11*, 19.
[7] Y. Yang, G. Zheng, Y. Cui, *Chem. Soc. Rev.* **2013**, *42*, 3018.
[8] S. Evers, L. F. Nazar, *Acc. Chem. Res.* **2013**, *46*, 1135.
[9] A. Manthiram, Y. Fu, Y.-S. Su, *Acc. Chem. Res.* **2013**, *46*, 1125.
[10] J. Wang, J. Yang, J. Xie, N. Xu, *Adv. Mater.* **2002**, *14*, 963.
[11] X. L. Ji, K. T. Lee, L. F. Nazar, *Nat. Mater.* **2009**, *8*, 500.
[12] B. Zhang, X. Qin, G. R. Li, X. P. Gao, *Energy Environ. Sci.* **2010**, *3*, 1531.
[13] J. C. Guo, Y. H. Xu, C. S. Wang, *Nano Lett.* **2011**, *11*, 4288.
[14] G. Zheng, Y. Yang, J. J. Cha, S. S. Hong, Y. Cui, *Nano Lett.* **2011**, *11*, 4463.
[15] N. Jayaprakash, J. Shen, S. S. Moganty, A. Corona, L. A. Archer, *Angew. Chem. Int. Ed.* **2011**, *50*, 5904.
[16] S. Xin, L. Gu, N.-H. Zhao, Y.-X. Yin, L.-J. Zhou, Y.-G. Guo, L.-J. Wan, *J. Am. Chem. Soc.* **2012**, *134*, 18510.
[17] S. Xin, Y.-X. Yin, L.-J. Wan, Y.-G. Guo, *Part. Part. Syst. Charact.* **2013**, *30*, 321.
[18] H. Ye, Y.-X. Yin, S. Xin, Y.-G. Guo, *J. Mater. Chem. A* **2013**, *1*, 6602.
[19] Y.-X. Yin, S. Xin, Y.-G. Guo, L.-J. Wan, *Angew. Chem. Int. Ed.* **2013**, *52*, 13186.
[20] J. Guo, Z. Yang, Y. Yu, H. D. Abruña, L. A. Archer, *J. Am. Chem. Soc.* **2013**, *135*, 763.
[21] Y. Su, A. Manthiram, *Nat. Commun.* **2013**, *3*, 1166.
[22] J. Kim, D.-J. Lee, H.-G. Jung, Y.-K. Sun, J. Hassoun, B. Scrosati, *Adv. Funct. Mater.* **2013**, *23*, 1076.

[23] Y. Fu, Y. Su, A. Manthiram, *Angew. Chem. Int. Ed.* **2013**, *52*, 6930.
[24] H. Wang, Y. Yang, Y. Liang, J. T. Robinson, Y. Li, A. Jackson, Y. Cui, H. Dai, *Nano Lett.* **2011**, *11*, 2644.
[25] L. Ji, M. Rao, H. Zheng, L. Zhang, Y. Li, W. Duan, J. Guo, E. J. Cairns, Y. Zhang, *J. Am. Chem. Soc.* **2011**, *133*, 18522.
[26] L. Xiao, Y. Cao, J. Xiao, B. Schwenzer, M. H. Engelhard, L. V. Saraf, Z. Nie, G. J. Exarhos, J. Liu, *Adv. Mater.* **2012**, *24*, 1176.
[27] Y. Su, Y. Fu, T. Cochell, A. Manthiram, *Nat. Commun.* **2013**, *4*, 2985.
[28] T. Yim, M.-S. Park, J.-S. Yu, K. J. Kim, K. Y. Im, J.-H. Kim, G. Jeong, Y. N. Jo, S.-G. Woo, K. S. Kang, I. Lee, Y.-J. Kim, *Electrochim. Acta* **2013**, *107*, 454.
[29] S. S. Zhang, *Electrochim. Acta* **2013**, *97*, 226.
[30] S. S. Zhang, *Front. Energy Res.* **2013**, *1*, 10.
[31] T. Fujimori, A. Morelo-Gómez, Z. Zhu, H. Muramatsu, R. Futamura, K. Urita, M. Terrones, T. Hayashi, M. Endo, S. Y. Hong, Y. C. Choi, D. Tománek, K. Kaneko, *Nat. Commun.* **2013**, *4*, 2162.
[32] X. Ji, S. Evers, R. Black, L. F. Nazar, *Nat. Commun.* **2011**, *2*, 325.
[33] J. Fanous, M. Wegner, J. Grimminger, Ä. Andresen, M. R. Buchmeiser, *Chem. Mater.* **2011**, *23*, 5024.
[34] Y. Yang, G. Zheng, S. Misra, J. Nelson, M. F. Toney, Y. Cui, *J. Am. Chem. Soc.* **2012**, *134*, 15387.
[35] C. Barchasz, F. Molton, C. Duboc, J.-C. Lepretre, S. P. Patoux, F. Alloin, *Anal. Chem.* **2012**, *84*, 3973.
[36] K. Cai, M.-K. Song, E. J. Cairns, Y. Zhang, *Nano Lett.* **2012**, *12*, 6474.
[37] W. J. Chung, J. J. Grebel, E. T. Kim, H. Yoon, A. G. Simmonds, H. J. Ji, P. T. Dirlam, R. S. Glass, J. J. Wie, N. A. Nguyen, B. W. Guralnick, J. Park, Á. Somogyi, P. Theato, M. E. Mackay, Y.-E. Sung, K. Char, J. Pyun, *Nat. Chem.* **2013**, *5*, 518.
[38] Z. W. Seh, W. Li, J. J. Cha, G. Zheng, Y. Yang, M. T. Mcdowell, P.-C. Hsu, Y. Cui, *Nat. Commun.* **2013**, *4*, 1331.
[39] Z. Lin, Z. Liu, W. Fu, N. J. Dudney, C. Liang, *Adv. Funct. Mater.* **2013**, *23*, 1064.
[40] B. Meyer, *Chem. Rev.* **1976**, *76*, 367.
[41] S. Tougaard, *J. Vac. Sci. Technol. A* **1987**, *5*, 1275.
[42] D. Xiong, J. C. Burns, A. J. Smith, N. Sinha, J. R. Dahn, *J. Electrochem. Soc.* **2011**, *158*, A1431.
[43] M. L. Gordin, F. Dai, S. Chen, T. Xu, J. Song, D. Tang, N. Azimi, Z. Zhang, D. Wang, *ACS Appl. Mater. Interfaces* **2014**, *6*, 8006.
[44] K. Xu, *Chem. Rev.* **2004**, *104*, 4303.
[45] K. Xu, U. Lee, S. Zhang, J. L. Allen, T. R. Jow, *Electrochem. Solid State Lett.* **2004**, *7*, A273.
[46] A. V. Naumkin, A. Kraut-Vass, S. W. Gaarenstroom, C. J. Powell, "NIST X-ray photoelectron spectroscopy database," *NIST Standard Reference Database 20, Version 4.1*, http://srdata.nist.gov/xps/ (accessed: September 15, 2012).
[47] H. Momose, H. Honbo, S. Takeuchi, K. Nishimura, T. Horiba, Y. Muranaka, Y. Kozono, H. Miyadera, *J. Power Sources* **1997**, *68*, 208.
[48] J. R. Dahn, R. Fong, M. J. Spoon, *Phys. Rev. B* **1990**, *42*, 6424.
[49] J. R. Dahn, *Phys. Rev. B* **1991**, *44*, 9170.
[50] R. Demir-Cakan, M. Morcrette, Gangulibabu, A. Guéguen, R. Dedryvére, J.-M. Tarascon, *Energy Environ. Sci.* **2013**, *6*, 176.
[51] L. Mi, Y. Chen, W. Wei, W. Chen, H. Hou, Z. Zheng, *RSC Adv.* **2013**, *3*, 17431.
[52] J. Xia, J. Jiao, B. Dai, W. Qiu, S. He, W. Qui, P. Shen, L. Chen, *RSC Adv.* **2013**, *3*, 6132.
[53] C. Lai, K. Huang, J. Cheng, C. Lee, B. Hwang, L. Chen, *J. Mater. Chem.* **2010**, *20*, 6638.
[54] L. Suo, Y.-S. Hu, H. Li, M. Armand, L. Chen, *Nat. Commun.* **2013**, *4*, 1481.